

Reducing Safety Interventions in Provably Safe Reinforcement Learning

Jakob Thumm¹, Guillaume Pelat¹, and Matthias Althoff¹

Abstract—Deep Reinforcement Learning (RL) has shown promise in addressing complex robotic challenges. In real-world applications, RL is often accompanied by failsafe controllers as a last resort to avoid catastrophic events. While necessary for safety, these interventions can result in undesirable behaviors, such as abrupt braking or aggressive steering. This paper proposes two safety intervention reduction methods: action replacement and projection, which change the agent’s action if it leads to an unsafe state. These approaches are compared to the state-of-the-art constrained RL on the OpenAI safety gym benchmark and a human-robot collaboration task. Our study demonstrates that the combination of our method with provably safe RL leads to high-performing policies with zero safety violations and a low number of failsafe interventions. Our versatile method can be applied to a wide range of real-world robotics tasks, while effectively improving safety without sacrificing task performance.

I. INTRODUCTION

A. Motivation

Reinforcement learning (RL) has emerged as a promising approach for solving complex tasks in a variety of robotics applications, such as manipulation [1]–[3], mobile robots [4]–[6], and autonomous driving [7]–[9]. Recent work has shown that safety can be guaranteed for RL agents using additional system knowledge [10]–[18]. However, implementing safety mechanisms can result in undesirable behavior, such as sudden braking or high torques, which can be uncomfortable for humans or demanding for robot hardware. In addition, bringing the system to an invariably safe state (ISS), e.g. a full stop through a failsafe maneuver, can lead to significant recovery times. Consequently, it is desirable to keep the number of safety interventions as low as possible.

We present two approaches, action replacement and projection that reduce the number of safety interventions required while maintaining high performance, as illustrated in Fig. 1. Both approaches, use reachability analysis to evaluate the agent’s proximity to obstacles in the future. We consider the agent’s action as temporarily unsafe if it could cause safety interventions. In our replacement approach, we replace these temporarily unsafe actions with randomized actions that move the robot further away from unsafe states. Our projection method replaces the temporarily unsafe actions with an action that lies nearby in Euclidean space. Both approaches are complemented with a safety shield that guarantees safety online at a high frequency. To our best knowledge, we are the first to propose a technique that can

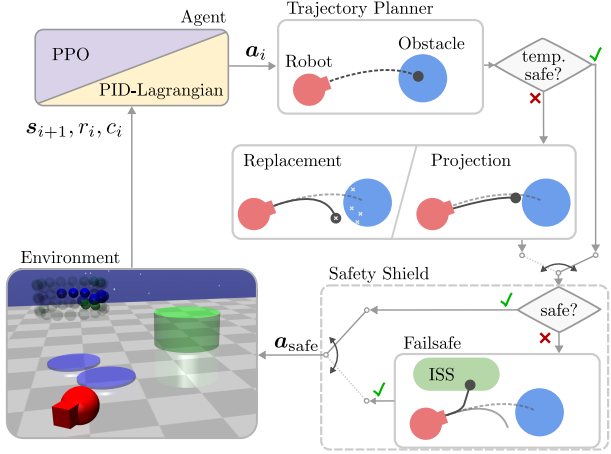


Fig. 1. Proposed intervention reduction technique: First, the agent generates an action a_i , which is then transformed into an intended trajectory via a trajectory planner. In case the intended trajectory would lead to a collision with an obstacle, we replace it with a temporarily safe trajectory using action replacement or projection. We verify the chosen trajectory during execution and fall back on a failsafe trajectory that ends in an invariably safe state (ISS) when needed.

significantly reduce the number of safety interventions in provably safe RL for any robotic environment. We compare our two approaches to constrained RL, which tries to solve the original RL problem while keeping the number of safety interventions below a predetermined threshold.

B. Contributions

Our contributions are fourfold. First, we introduce the first RL agent to the OpenAI safety gym [19] that guarantees zero constraint violations. Second, we propose two approaches that significantly reduce the number of failsafe interventions in safe RL, and compare it to constrained RL. Third, we evaluate our proposed approaches in the OpenAI safety gym and a human-robot collaboration task. Finally, we demonstrate the real-world impact of our proposed method on a six degree-of-freedom (DoF) manipulator in a human environment¹.

C. Related work

The safety of RL agents has been a major concern since the introduction of RL and deep RL [20], [21]. To broadly categorize safe RL, Brunke et al. [22] classify safe RL methods according to their types of constraints, which include soft constraints, probabilistic constraints, and hard constraints.

¹The authors are with the School of Informatics, Technical University of Munich, 85748 Garching, Germany. {jakob.thumm, guillaume.pelat, althoff}@tum.de

¹<https://youtu.be/dIvhvV5z8bM>

This work does not rely on probabilistic constraint methods, so readers interested in this topic are referred to [22]. The most common soft constraint method is constrained RL, which aims to learn the policy with the highest reward while limiting the number of constraint violations [20]. The Lagrangian method [20] is a popular way to address constrained RL problems by converting them to a dual problem, following constrained optimization theory [23, Chapter 5] and optimizing the Lagrangian multiplier in conjunction with the RL policy. More recent works, such as constrained policy optimization [24], constrained RL with a PID-controlled Lagrange multiplier (PID-Lagrangian) [25], and worst-case soft actor-critic [26] build on the Lagrangian method and make it applicable to deep RL. A drawback of constrained RL is that it cannot guarantee safety in a provable way, as the learned behavior is not formalized or proven. Additionally, most constrained RL methods have a non-zero constraint violation threshold, making it impossible to ensure safety with complete certainty.

Hard constraint methods can guarantee the safety of an agent at all times, leading to provably safe RL. Provably safe RL can be categorized into three types based on the methods used to alter the agent's actions [27]: action replacement [11], [16], [28], [29], action projection [13], [14], [30], [31], and action masking [12], [15], [32]. However, both action projection and replacement can cause strong interventions with the negative effects mentioned earlier. To address this issue, some works have used a negative reward to penalize safety interventions [11], [13], [16]. Nonetheless, this approach requires careful hand-tuning and often results in either no reduction of interventions or significant performance loss, as we will discuss in more detail later. In order to evaluate the effectiveness of safe RL methods, the OpenAI safety gym [19] has become a widely used benchmark, offering a range of tasks that require balancing performance and safety considerations.

D. Article structure

Sec. II a) defines the problem to solve, b) introduces the necessary notation for the RL approaches and reachability analysis, and d) formalizes a generalization of our previously introduced safety shield to general robot environments. We then present how the number of failsafe interventions can be reduced in Sec. III. Sec. IV discusses the main results of our experiments. Finally, we conclude this article and give an outlook on future work in Sec. V.

II. PRELIMINARIES

A. Problem statement

In this work, we address the problem of safe reach-avoid robotic tasks in environments with both static and dynamic obstacles. Specifically, the robot's objective is to reach a target position while avoiding collisions with obstacles. The safety of the robot and the environment have to be ensured. Our goal is to minimize the number of safety interventions to promote natural and interference-free behavior of the robot.

B. Reinforcement learning

RL aims to find an optimal policy for Markov decision processes (MDPs), which are defined by the tuple $(\mathcal{S}, \mathcal{A}, R, p, \gamma)$ [33]. In this work, we focus on continuous state \mathcal{S} and action spaces \mathcal{A} . We define the state-transition probability density function $p : \mathcal{S} \times \mathcal{S} \times \mathcal{A} \rightarrow [0, \infty)$ to describe the probability of reaching the next state s_{i+1} when choosing action a_i in state s_i . The environment provides a reward $R : \mathcal{S} \times \mathcal{S} \times \mathcal{A} \rightarrow \mathbb{R}$ for each transition, which is discounted by the discount factor γ . The agent learns a stochastic policy $\pi(a_i | s_i)$ from which action a_i is sampled in state s_i .

For constrained RL, Altman [20] extends the MDP by a cost function $C : \mathcal{S} \times \mathcal{S} \times \mathcal{A} \rightarrow \mathbb{R}$, a cost limit $d : \mathcal{S} \times \mathcal{A} \rightarrow \mathbb{R}$, and a cost discount γ_C . In practice, we limit ourselves to a fixed cost limit $d \in \mathbb{R}$. The optimization objective for the policy π of maximizing the expected sum of discounted rewards $J(\pi) = \mathbb{E} [\sum_{t=0}^{\infty} \gamma^t R(s_i, a_i, s_{i+1})]$ is then complemented with the constraint of a limited expected sum of discounted costs $J_C(\pi) = \mathbb{E} [\sum_{i=0}^{\infty} \gamma_C^i C(s_i, a_i, s_{i+1})] \leq d$, where we assume a_i , s_{i+1} , and s_0 to be distributed according to $a_i \sim \pi$, $s_{i+1} \sim p$, $s_0 \sim \mathcal{S}_0$, and \mathcal{S}_0 is the set of initial states.

C. Reachability analysis

In this work, we adopt a reachability analysis approach for ensuring safety and finding low-interfering actions. Our considered systems follow the dynamics $\dot{x}(t) = f(x(t), u(t), w(t))$, with bounded control inputs $u \in \mathcal{U}$, disturbances $w \in \mathcal{W}$, and possible states $x \in \mathcal{X}$. We denote the control input sequence in the time interval $[t_0, t]$ as $u([t_0, t])$ and adopt this notation for all signals. Given such a control input sequence, an initial state x_0 , and a disturbance sequence $w([t_0, t])$, the system follows the trajectory $\chi(t, x_0, u([t_0, t]), w([t_0, t]))$. The forward reachable set $\mathcal{R}(t)$ of a system starting in the set of initial states \mathcal{X}_0 with unknown control inputs comprises all states reachable at time t :

$$\mathcal{R}(t) = \{\chi(t, x_0, u([t_0, t]), w([t_0, t])) \mid x_0 \in \mathcal{X}_0, \forall t : u(t) \in \mathcal{U}, w(t) \in \mathcal{W}\}. \quad (1)$$

An input signal can also be generated by a state-feedback control law $u_{\Phi_Z}(t) = \Phi_Z(x(t))$, resulting in the trajectory $\chi_Z(t, x_0, u_{\Phi_Z}(t)([t_0, t]), w([t_0, t]))$. The reachable set under a feedback controller is denoted by $\mathcal{R}_Z(t)$ and it is a subset of the reachable set with unknown control inputs

$$\mathcal{R}_Z(t) = \{\chi_Z(t, x_0, u_{\Phi_Z}([t_0, t]), w([t_0, t])) \mid x_0 \in \mathcal{X}_0, \forall t : w(t) \in \mathcal{W} \subseteq \mathcal{R}(t)\}. \quad (2)$$

All states reachable during the time interval $[t_0, t_1]$ are given by $\mathcal{R}([t_0, t_1]) = \bigcup_{t \in [t_0, t_1]} \mathcal{R}(t)$. We denote the set of points that a system can occupy in Euclidean space at time t and a time interval by $\mathcal{O}(\mathcal{R}(t))$ and $\mathcal{O}(\mathcal{R}([t_0, t_1]))$, respectively, and further refer to it as reachable occupancy (RO). We further introduce a point in Euclidean space as p , a ball as $\mathcal{B}(c, r) = \{p \mid \|p - c\|_2 \leq r\}$ with center c and radius r , and a function that overapproximates a RO with a ball ball $(\mathcal{O}) = \hat{\mathcal{B}}(c, R)$ so that $p \in \mathcal{O} \rightarrow p \in \hat{\mathcal{B}}(\mathcal{O})$.

D. Safety shield

In order to ensure safety of our RL agents, we utilize the safety shield for manipulators proposed in [18], and generalize it for arbitrary robotic environments. The safety shield relies on the existence of an ISS that can be reached from any state. Examples of an ISS include a fully stopped robot for manipulators or mobile robots, in accordance with the ISO 10218-1 2021 [34], and a state in which a formally-correct adaptive cruise controller for autonomous highway driving can be engaged [35]. As we demonstrated in [18], a safety shield for RL is less restrictive when it operates on a higher frequency than the RL agent’s action output. We therefore execute each RL action a_i for L time steps and perform a safety shield update at every time step.

At each time step k , we calculate an intended and a failsafe trajectory. Without loss of generality, we always reset the clock to t_0 at each time step. The intended trajectory χ_I follows the desired agent action output $\Phi_I(x(t), a)$ for L time steps, while the failsafe trajectory χ_F leads the robot to an ISS using a failsafe controller $\Phi_F(x(t))$ in k_{failsafe} time steps. We append a full failsafe trajectory to a single step of the intended trajectory to form a so-called shielded trajectory

$$\chi_S = \begin{cases} \chi_I(t, x_0, \mathbf{u}_{\Phi_I}([t_0, t]), \mathbf{w}([t_0, t])), & t \in [t_0, t_D] \\ \chi_F(t, x_1, \mathbf{u}_{\Phi_F}([t_D, t]), \mathbf{w}([t_D, t])), & t \in [t_D, t_S], \end{cases} \quad (3)$$

with $D = 1$, t_S as the time of the end of the shielded trajectory, and $S = D + k_{\text{failsafe}}$.

We verify the shielded trajectory by calculating the ROs of the robot $\mathcal{O}^{(r)}(\mathcal{R}_S^{(r)}([t_0, t_S]))$ and the J obstacles $\mathcal{O}^{(o)} = \bigcup_{j \in J} \mathcal{O}^{(o_j)}(\mathcal{R}^{(o_j)}([t_0, t_S]))$ in the time interval $[t_0, t_S]$. We then check if the ROs are intersection-free with our open-source toolbox SaRA [36]:

$$\mathcal{O}^{(r)} \cap \mathcal{O}^{(o)} = \emptyset. \quad (4)$$

If the verification fails, we can safely execute the last verified failsafe trajectory. We assume the robot to start from an ISS, allowing us to ensure safety indefinitely through induction. The set-based representation of the systems enables us to guarantee safety in both simulation and real-world applications, thus bridging the simulation-to-reality gap. For a detailed implementation of our safety shield for the OpenAI safety gym, please refer to the Appendix.

III. METHODOLOGY

In this work, we investigate four methods for reducing the number of failsafe interventions. The state-of-the-art method is to assign a fixed negative reward when the failsafe is triggered in an RL step [11], [13], [16]. However, our evaluation in Fig. 2 shows that this approach often results in either no improvement in the number of failsafe interventions or a drastic reduction in performance. To improve on this approach, we introduce two safety reduction techniques, action replacement and projection, and compare it with constrained RL.

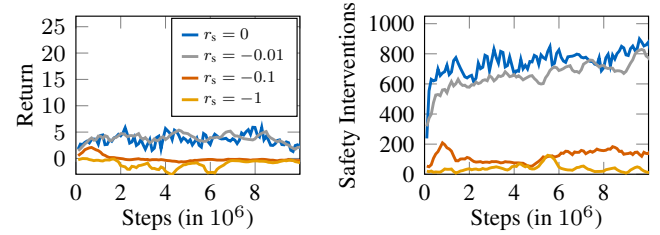


Fig. 2. Reward and shield activation for different values of reward punishment r_s for shield usage with the shielded PPO agent. If the reward punishment is too weak ($r_s = -0.01$), the shield usage is not affected, and if it is slightly too high ($r_s = -0.1$), the agent learns to never use the shield at all cost.

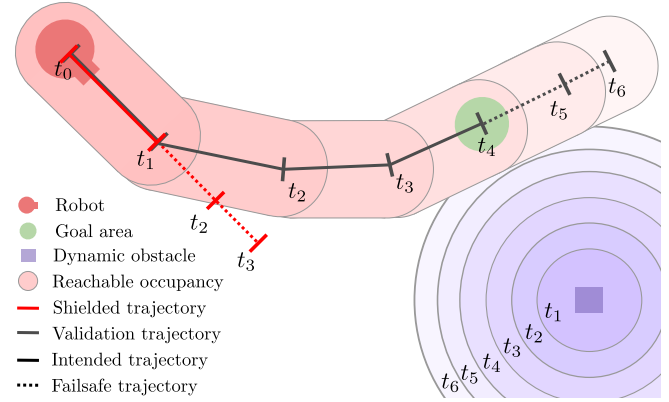


Fig. 3. The four types of trajectories in the replacement approach. The intended trajectory resembles the agent’s action. The failsafe trajectory is appended to a single step of the intended trajectory to build a shielded trajectory. The agent’s action is validated based on the validation trajectory consisting of the entire intended trajectory and a subsequent failsafe trajectory. In this example, the shielded trajectory is safe, but the agent’s action needs to be replaced as the validation trajectory collides with the reachable set of the dynamic obstacle.

A. Action replacement

Our first approach replaces actions that result in an intersection between the reachable occupancies of robot and obstacles, with a temporarily safe action. We want to highlight that the safety of this temporarily safe action is still guaranteed online by the safety shield as described in Sec. II-D. Unlike our safety shield method, verifying the shielded trajectory in the beginning of the RL step is insufficient since a collision could occur at any time during the RL step. Thus, to prevent interventions during the RL step, we construct a validation trajectory χ_V as depicted in Fig. 3, which is composed of the entire intended trajectory of the RL step followed by a failsafe trajectory. The validation trajectory can be defined in accordance to (3) with $D = L$. After constructing the validation trajectory, we validate it for temporary safety by checking for intersections with the robot’s reachable occupancies in the time interval $[t_0, t_V]$ as in (4).

If the validation fails, we iteratively sample M replacement actions uniformly from the action space and generate the corresponding validation trajectories for each action. We

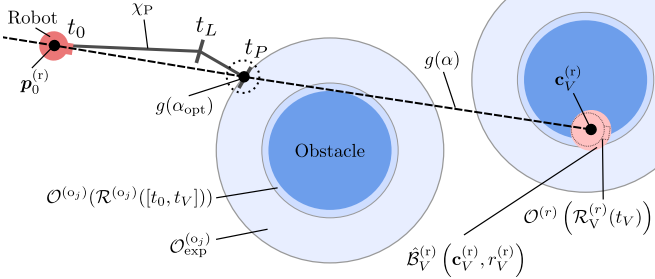


Fig. 4. Our action projection method finds the longest intersection-free line segment from the current robot position to the end of the validation trajectory.

then check these validation trajectories for intersection with the environment as described above. The agent then executes the first temporarily safe replacement action found during the RL step. If no temporarily safe action is found in M samples, we execute a zero action, for which safety is also ensured as described in Sec. II-D. As a result, the action replacement method cannot prevent all safety interventions in practice, but reduces the number of failsafe interventions significantly as shown in our experiments in Sec. IV.

B. Action projection

Our second intervention reduction approach is an action projection. The goal is to find a reachable point in space near the position of the robot at the end of the intended trajectory without colliding with the environment, as illustrated in Fig. 4. We first calculate the spherical overapproximation of the reachable occupancy of the robot at the end of the validation trajectory $\hat{B}_V^{(r)}(c_V^{(r)}, r_V^{(r)}) = \text{ball}(\mathcal{O}^{(r)}(R_V^{(r)}(t_V)))$. Next, we construct a straight line from the current robot position to the predicted end of the validation trajectory as

$$g(\alpha) = p_0^{(r)} + \alpha (c_V^{(r)} - p_0^{(r)}), \alpha \in \mathbb{R}, \quad (5)$$

where $p_0^{(r)}$ is the center of the set of possible robot positions at the beginning of a time step. The reachable occupancies of the obstacles in the time interval $[t_0, t_V]$ are then expanded by $r_{\text{exp}} = r_V^{(r)} + \epsilon$ using

$$\mathcal{O}_{\text{exp}}^{(o)} = \bigcup_{j \in J} \mathcal{O}^{(o_j)}(\mathcal{R}^{(o_j)}([t_0, t_V])) \oplus \mathcal{B}(\mathbf{0}, r_{\text{exp}}), \quad (6)$$

where \oplus is the Minkowski sum². We look for the longest intersection-free line segment on g with $\mathcal{G}([\alpha_1, \alpha_2]) = \{g(\alpha) \mid \alpha \in [\alpha_1, \alpha_2]\}$ from the current robot position to $c_V^{(r)}$ using

$$\begin{aligned} \max & \quad \alpha_{\text{opt}} \\ \text{subject to} & \quad \mathcal{G}([0, \alpha_{\text{opt}}]) \bigcap \mathcal{O}_{\text{exp}}^{(o)} = \emptyset, \\ & \quad \alpha_{\text{opt}} < 1 \\ & \quad -\alpha_{\text{opt}} < \alpha_{\text{opt, min}}, \end{aligned} \quad (7)$$

² $\mathcal{A} \oplus \mathcal{B} = \{a + v \mid a \in \mathcal{A}, v \in \mathcal{B}\}$

where we adapt $\alpha_{\text{opt, min}}$ to the robot dynamics. Finally, we use a trajectory planner to plan a trajectory χ_P from $p_0^{(r)}$ to an ISS in an ϵ -bound around $c_V^{(r)}$, which ensures that the first L steps of the trajectory have a constant control input. As the projection only checks against intersection in the end-configuration of the validation trajectory, it is not guaranteed that the resulting projected trajectory is intersection-free in (4). Therefore, if χ_P would result in an intersection, we can repetitively reduce α for M times to find a more conservative projection point. If no temporarily safe trajectory χ_P can be found, we execute the zero action and continue to ensure safety with our safety shield.

C. Constrained RL

We compare the two presented methods with a constrained RL approach that aims to minimize the number of failsafe interventions. We assign a cost of 1 to each failsafe intervention in an RL step and train a PID-Lagrangian agent to perform the environment task while staying below a threshold of safety interventions. This approach minimizes safety interventions without any additional implementation effort.

IV. EXPERIMENTS

A. OpenAI safety gym

In our OpenAI safety gym experiments, we evaluate the proposed safety reduction methods on two continuous control tasks: Point-Goal and Point-Button. For both tasks, we consider a cylindrical robot modelled as a point mass that can act on its acceleration in the direction of heading and yaw rate. The agent perceives its velocity, acceleration, and distance to the target and obstacle through a velocity, an acceleration, and a LiDAR sensor respectively. Each episode of a task starts with randomized positions of the robot, obstacles, and goal. The Point-Goal task requires the agent to navigate to a target area while avoiding hazards and vases, which can be pushed around by the agent. On the other hand, in the Point-Button task, the agent needs to move to the correct button from multiple options while avoiding dynamic obstacles called gremlins. For both tasks, the agent incurs a cost of 1 for being in a hazard or an incorrect button area, as well as for colliding with a vase or a gremlin. To increase the challenge for the agent, both tasks have two levels of difficulty, with level 2 featuring a higher number of obstacles. Each episode lasts for 1000 RL steps, with a new goal being randomly selected upon completion. All training results in Fig. 5 show the performance over 2 million RL steps on 3 random seeds. We kept the hyperparameters from [25] fix for all training runs on every environment.

In the Point-Button environments, we encounter a complication with the assumption that a stopped robot is in an invariant safe state (ISS). Specifically, the challenge arises when the robot steps on a button, causing it to immediately switch from being the goal button to an incorrect button. Consequently, halting the robot on the button is no longer adequate to ensure safety. Given this limitation, we opted

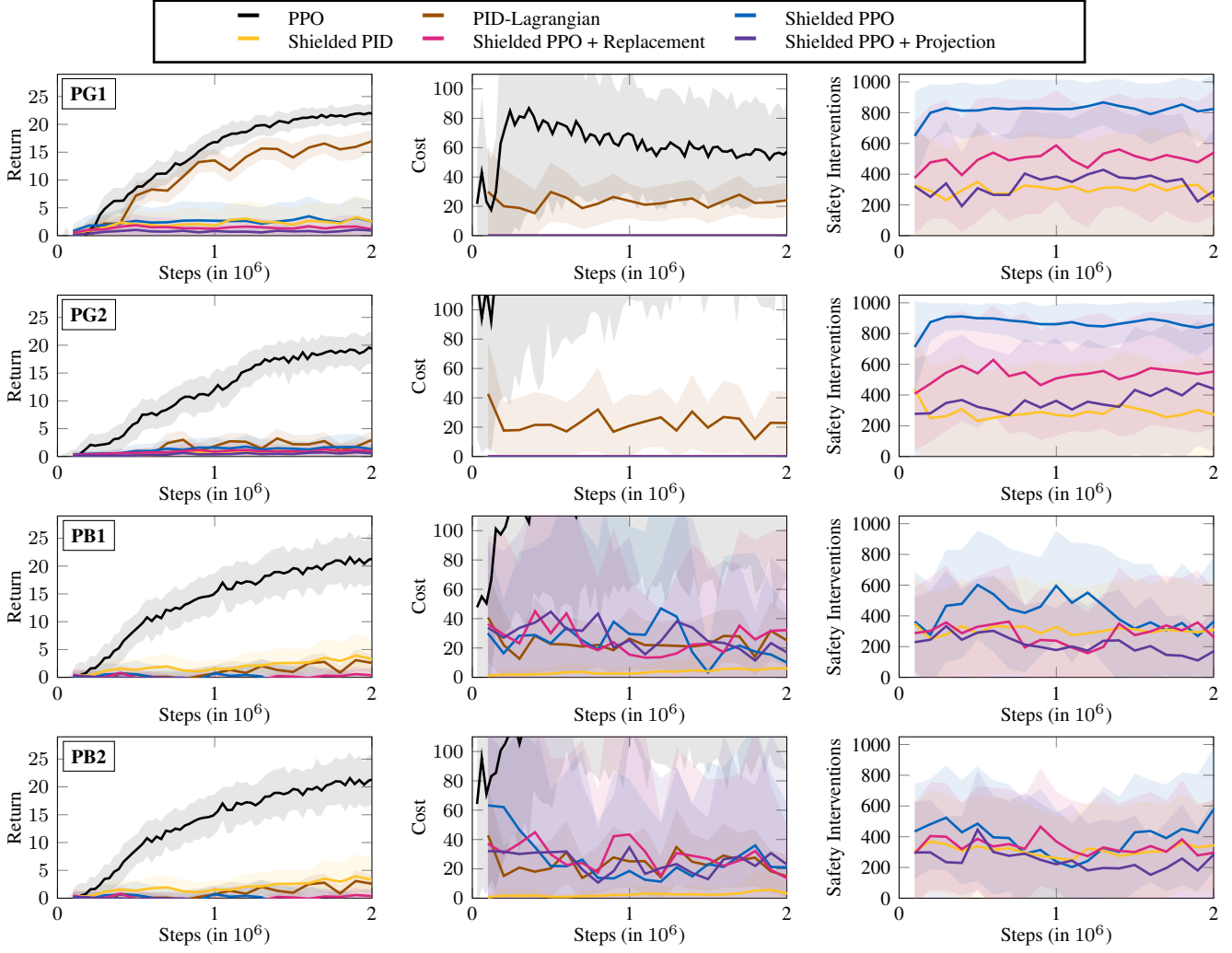


Fig. 5. Mean and standard deviation over 3 random seeds for the OpenAI safety gym environments. From top to bottom: Point-Goal1, Point-Goal2, Point-Button1, and Point-Button2. From left to right: the return, cost, and number of safety interventions per episode with length 1000. Our shielded PID Lagrangian methods show a significantly lower cost than the baselines PPO and PID-Lagrangian while maintaining competitive returns in all but the Point-Goal1 environment. The costs for the shielded agents in the Button environments are non-zero because we did not account for incorrectly pushed buttons. There are no other collisions with the static environment or the gremlins. PID-Lagrangian reduces the number of failsafe interventions in the Goal environments drastically.

to exclude buttons from our safety shield and test the capabilities of PID-Lagrangian to reduce two types of constraint violations simultaneously.

Our results in Fig. 5 demonstrate the effectiveness of our safety shield in mitigating all environment costs in the Point-Goal tasks, and all but the button costs in the Point-Button task, serving as the first provably safe benchmark in the OpenAI safety gym. Our action projection method significantly reduces failsafe interventions of the shielded PPO agent across all environments, while the action replacement method is less effective in reducing safety interventions due to its failure to find a valid replacement action. Notably, the reduction of failsafe interventions using either approach does not have a significant impact on the shielded PPO agent’s performance. The shielded PID-Lagrangian agent performs well in the Point-Button environments, outperforming previous safe RL methods, and effectively re-

duces the remaining button costs that our safety shield could not prevent. In the Point-Goal tasks, PID-Lagrangian can also reduce the number of failsafe interventions, although the cost threshold is an important hyperparameter to tune.

B. Human-robot collaboration

To test the transferability of our findings to more complex robotics tasks, we trained a reaching task in a human-robot simulation and then deployed the resulting agents on a Schunk LWA 4P manipulator in a real-world setting. Our six DoF manipulator is tasked with moving from a given initial end-effector position p_{init} to a target end-effector position p_{goal} , with the episode terminating upon goal achievement. The RL agent receives two types of observations: the difference between the target and current end-effector position, and the distance between the end-effector and the human head, i.e., $s = [(p_{\text{goal}} - p_{\text{eff}})^\top, |p_{\text{eff}} - p_{\text{head}}|]$. The agent’s

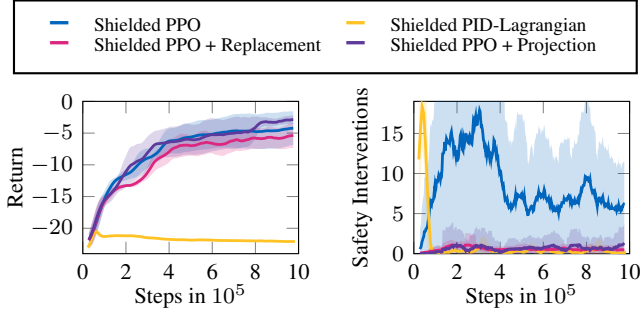


Fig. 6. Mean and standard deviation of cumulative reward and failsafe interventions per episode over 3 random seeds for the human-robot collaboration environment with 1 million RL steps and 200 RL steps per episode.

actions are specified as the change in end-effector positions from the current position p_{eff} to the next position p_{next} , i.e., $p_{\text{next}} = p_{\text{eff},i} + a_i$. Our action projection technique is only applied to the RO of the end-effector, as the ball enclosure of the entire robot would be too conservative. The human in the environment follows pre-recorded animations, but its position is randomized at the start of each episode. As safety is paramount in human environments, we only compare the shielded agents, and refer to [18] for a detailed comparison with unsafe agents.

Fig. 6 shows that the shielded PPO agent performs well in the reaching task, but triggers a failsafe intervention in 2.5% of the RL steps, with up to 7.5% at the beginning of the training. Our proposed failsafe prevention techniques reduce the number of safety interventions by a factor of 10 to around 0.25%, with no decrease in performance. The replacement method achieves slightly better failsafe reduction than the action projection, but at the cost of lower performance. Contrary to the OpenAI safety gym environment, the PID-Lagrangian agent is unable to learn a suitable policy that is both high-performing and reduces failsafe interventions, even after exhaustive hyperparameter optimization. We attribute the limited success of PID-Lagrangian to the increased complexity of the human-robot environment. We also present the performance of our agents on a real-world robot in our supplementary video. The shielded PPO agent consistently fulfills the task, while the action replacement and projection techniques allow the agent to move away from the human RO, resulting in smoother trajectories and fewer safety interventions.

V. CONCLUSIONS

Our provably safe benchmark for the OpenAI safety gym achieved competitive performance, with zero safety violations on the Point-Goal and almost zero violations on the Point-Button tasks. Our evaluation demonstrated that a reward punishment for safety interventions is often insufficient for reducing their number due to the high sensitivity of the agent’s performance to the reward. Despite the shielded PID-Lagrangian agent showed promising results in the OpenAI safety gym, it failed to learn a viable policy in our more complex human-robot collaboration task. On the other hand,

our proposed action projection method can prevent close to all failsafe interventions without performance sacrifices. We conclude that our provably safe shielded PPO agent with action projection is best suited for a wide variety of real-world safety-critical robotics tasks. Our supplementary video showcases the effectiveness of our approach in a real-world manipulation setting.

In our future work, we aim to extend the applicability of our projection method to more complex robot geometries, including non-spherical robots. One potential direction is to design the projection to include points outside the constructed line from the current robot position to the target position of the action. This would allow for a more flexible projection that can better account for potential obstacles in the robot’s path. Additionally, we plan to investigate advanced action sampling methods to improve the effectiveness of our action replacement approach. To further demonstrate the effectiveness of our safety shield, we intend to test it in more challenging real-world human-robot collaboration environments, such as construction sites or manufacturing facilities. These environments pose additional safety challenges due to the presence of heavy machinery and high-risk tasks, and thus provide an opportunity to evaluate the robustness of our approach.

APPENDIX

A. Adaptions to safety shield for point robot

In the OpenAI safety gym, we consider a robot modelled as a point mass, whose state can be described by its position $\mathbf{p}^\top = [p_x, p_y]$, velocity $\mathbf{v}^\top = [v_x, v_y]$, and orientation φ , i.e., $\mathbf{x} = [p_x, p_y, v_x, v_y, \varphi]^\top$. The robot has two actuators $\mathbf{u} = [u_1, u_2]$. The non-linear system dynamics are given by

$$\dot{\varphi} = u_2 \quad (8a)$$

$$\dot{\mathbf{v}} = \mathbf{R}_z(\varphi) [u_1, 0]^\top \quad (8b)$$

$$\dot{\mathbf{p}} = \mathbf{v}, \quad (8c)$$

where $\mathbf{R}_z(\varphi)$ describes the rotation matrix around the z-axis with angle φ . The input is limited by $|u_1| \leq u_{1,\text{max}} = 0.05/m$ and $|u_2| \leq u_{2,\text{max}} = 0.05/m$, where m is the mass of the robot. It is important to note that the robot dynamics are only approximated by these equations and do not necessarily reflect the physical behavior of a real-world robot.

The intended trajectory can be directly obtained from (8). For the failsafe trajectory, we first rotate the robot so that its orientation aligns with its direction of travel $\arctan(v_y/v_x) \approx \varphi$. The robot is then braked in the direction of travel with $u_1 = -\text{sign}(\cos(\varphi)v_x + \sin(\varphi)v_y) \cdot u_{1,\text{max}}$.

For the reachability analysis, we consider the OpenAI safety gym as a two-dimensional environment. The reachable occupancies of the obstacles are calculated using the velocity-constrained model proposed by Liu et al. [37]. To calculate the reachable occupancy of the point robot, only the position is relevant, so we define its trajectory with abuse of notation as the solution of (8c)

$\chi_{\mathbf{p}}(t, \mathbf{x}_0, \mathbf{u}([t_0, t]), \mathbf{w}([t_0, t]))$. To achieve fast calculation times, we linearly interpolate the trajectory of the robot between two shield steps t_0 and t_1 as

$$\tilde{\chi}_{\mathbf{p}}(t, \mathbf{x}_0, \mathbf{u}([t_0, t]), \mathbf{w}([t_0, t])) = \xi \mathbf{p}(t_0) + (1 - \xi) \mathbf{p}(t_1), \quad (9)$$

with $\xi \in [0, 1]$. The resulting linearization error in the position can be over-approximated by

$$\zeta = \left| \tilde{\chi}_{\mathbf{p}}\left(\frac{t_1 + t_0}{2}\right) - \chi_{\mathbf{p}}\left(\frac{t_1 + t_0}{2}\right) \right| \leq \frac{d^2 p(t)}{dt^2} \frac{(\Delta t)^2}{8}, \quad (10)$$

as shown by Beckert et al. [38]. For the point robot, this results in $\zeta = \frac{a_{0,\max}(\Delta t)^2}{8m}$. The reachable set of the position of the robot is therefore

$$\mathcal{R}_{\mathbf{p}}(t) = ((1 - \xi(t))\mathbf{p}(t_0) + \xi(t)\mathbf{p}(t_1)) \oplus \mathcal{B}(\mathbf{0}, \zeta), \quad (11)$$

where $\xi(t) = \frac{t_1 - t}{t_1 - t_0}$. To get the reachable occupancy of the robot, we simply add its radius $r^{(r)}$ to the reachable set

$$\mathcal{O}^{(r)}(\mathcal{R}_{\mathbf{p}}(t)) = \mathcal{R}_{\mathbf{p}}(t) \oplus \mathcal{B}(\mathbf{0}, r^{(r)}). \quad (12)$$

The linearization in (9) simplifies the reachable occupancy of the robot between two shield steps to a capsule, which allows for fast intersection checking with the environment.

The OpenAI safety gym only provides lidar measurements of the obstacles, which can result in occlusions of obstacles by other obstacles. Such occlusions can be handled using set-based predictions as shown exemplary for an autonomous driving task in [39]. However, this solution increases the size of the reachable sets, making the safety shield more restrictive. To mitigate this issue, we decided to augment the safety shield with precise information about the exact position of each obstacle. The RL agent, however, does not have access to this information, ensuring a fair comparison with the benchmark.

ACKNOWLEDGMENT

The authors gratefully acknowledge financial support by the Horizon 2020 EU Framework Project CONCERT under grant 101016007.

REFERENCES

- [1] T. P. Lillicrap, J. J. Hunt, A. Pritzel, N. Heess, T. Erez, Y. Tassa, D. Silver, and D. Wierstra, “Continuous control with deep reinforcement learning,” ser. Proc. of the 4th Int. Conf. on Learning Representations (ICLR), 2016.
- [2] O. M. Andrychowicz, B. Baker, M. Chociej, R. Józefowicz, B. McGrew, J. Pachocki, A. Petron, M. Plappert, G. Powell, A. Ray, J. Schneider, S. Sidor, J. Tobin, P. Welinder, L. Weng, and W. Zaremba, “Learning dexterous in-hand manipulation,” *International Journal of Robotics Research*, vol. 39, no. 1, pp. 3–20, 2020.
- [3] R. Liu, F. Nageotte, P. Zanne, M. de Mathelin, and B. Dresp-Langley, “Deep reinforcement learning for the control of robotic manipulation: A focussed mini-review,” *Robotics*, vol. 10, no. 1, pp. 1–13, 2021.
- [4] L. Tai, G. Paolo, and M. Liu, “Virtual-to-real deep reinforcement learning: Continuous control of mobile robots for mapless navigation,” in *Proc. of the IEEE/RSJ Int. Conf. on Intelligent Robots and Systems (IROS)*, 2017, pp. 31–36.
- [5] K. Zhu and T. Zhang, “Deep reinforcement learning based mobile robot navigation: A review,” *Tsinghua Science and Technology*, vol. 26, no. 5, pp. 674–691, 2021.
- [6] L. Chang, L. Shan, C. Jiang, and Y. Dai, “Reinforcement based mobile robot path planning with improved dynamic window approach in unknown environment,” *Autonomous Robots*, vol. 45, no. 1, pp. 51–76, 2021.
- [7] A. El Sallab, M. Abdou, E. Perot, and S. Yogamani, “Deep reinforcement learning framework for autonomous driving,” *Proc. of the IS&T Int. Symp. on Electronic Imaging (EI): Autonomous Vehicles and Machines*, pp. 70–76, 2017.
- [8] X. Wang, H. Krasowski, and M. Althoff, “Commonroad-rl: A configurable reinforcement learning environment for motion planning of autonomous vehicles,” in *IEEE Int. Intelligent Transportation Systems Conf. (ITSC)*, 2021, pp. 466–472.
- [9] B. R. Kiran, I. Sobh, V. Talpaert, P. Mannion, A. A. A. Sallab, S. Yogamani, and P. Pérez, “Deep reinforcement learning for autonomous driving: A survey,” *IEEE Transactions on Intelligent Transportation Systems*, vol. 23, no. 6, pp. 4909–4926, 2022.
- [10] F. Berkenkamp, M. Turchetta, A. P. Schoellig, and A. Krause, “Safe model-based reinforcement learning with stability guarantees,” in *Proc. of the 31st Int. Conf. on Neural Information Processing Systems*, ser. NIPS’17, 2017, pp. 908–919.
- [11] M. Alshiekh, R. Bloem, R. Ehlers, B. Könighofer, S. Niekum, and U. Topcu, “Safe reinforcement learning via shielding,” in *Proc. of the 32nd AAAI Conf. on Artificial Intelligence (AAAI)*, 2018.
- [12] N. Fulton and A. Platzer, “Safe reinforcement learning via formal methods: Toward safe control through proof and learning,” *Proc. of the 32nd AAAI Conf. on Artificial Intelligence (AAAI)*, Apr. 2018.
- [13] T.-H. Pham, G. De Magistris, and R. Tachibana, “Optplayer - practical constrained optimization for deep reinforcement learning in the real world,” in *Proc. of the IEEE Int. Conf. on Robotics and Automation (ICRA)*, 2018, pp. 6236–6243.
- [14] R. Cheng, G. Orosz, R. M. Murray, and J. W. Burdick, “End-to-end safe reinforcement learning through barrier functions for safety-critical continuous control tasks,” *Proc. of the AAAI Conf. on Artificial Intelligence*, vol. 33, no. 01, pp. 3387–3395, Jul. 2019.
- [15] H. Krasowski, X. Wang, and M. Althoff, “Safe reinforcement learning for autonomous lane changing using set-based prediction,” in *Proc. of the IEEE 23rd Int. Conf. on Intelligent Transportation Systems (ITSC)*, 2020, pp. 1–7.
- [16] Y. S. Shao, C. Chen, S. Kousik, and R. Vasudevan, “Reachability-based trajectory safeguard (rts): A safe and fast reinforcement learning safety layer for continuous control,” *IEEE Robotics and Automation Letters*, vol. 6, no. 2, pp. 3663–3670, 2021.
- [17] N. Hunt, N. Fulton, S. Magliacane, T. N. Hoang, S. Das, and A. Solar-Lezama, “Verifiably safe exploration for end-to-end reinforcement learning,” in *Proc. of the 24th Int. Conf. on Hybrid Systems: Computation and Control (HSCC)*, 2021.
- [18] J. Thumm and M. Althoff, “Provably safe deep reinforcement learning for robotic manipulation in human environments,” in *Proc. of the IEEE Int. Conf. on Robotics and Automation (ICRA)*, 2022, pp. 6344–6350.
- [19] A. Ray, J. Achiam, and D. Amodei, “Benchmarking safe exploration in deep reinforcement learning,” *arXiv preprint arXiv:1910.01708*, vol. 7, 2019.
- [20] E. Altman, “Constrained markov decision processes with total cost criteria: Lagrangian approach and dual linear program,” *Mathematical Methods of Operations Research*, vol. 48, no. 3, pp. 387–417, Dec. 1998.
- [21] J. García and F. Fernández, “A comprehensive survey on safe reinforcement learning,” *Journal of Machine Learning Research*, vol. 16, no. 1, pp. 1437–1480, 2015.
- [22] L. Brunke, M. Greeff, A. W. Hall, Z. Yuan, S. Zhou, J. Panerati, and A. P. Schoellig, “Safe learning in robotics: From learning-based control to safe reinforcement learning,” *Annual Review of Control, Robotics, and Autonomous Systems*, vol. 5, no. 1, pp. 411–444, 2022.
- [23] S. Boyd, S. P. Boyd, and L. Vandenberghe, *Convex optimization*. Cambridge university press, 2004.
- [24] J. Achiam, D. Held, A. Tamar, and P. Abbeel, “Constrained policy optimization,” in *Proc. of the 34th Int. Conf. on Machine Learning (ICML)*, 2017, pp. 22–31.
- [25] A. Stooke, J. Achiam, and P. Abbeel, “Responsive safety in reinforcement learning by pid lagrangian methods,” in *Proc. of the 37th Int. Conf. on Machine Learning*, vol. 119. PMLR, Jul. 2020, pp. 9133–9143.
- [26] Q. Yang, T. D. Simão, S. H. Tindemans, and M. T. J. Spaan, “Wcsac: Worst-case soft actor critic for safety-constrained reinforcement

learning.” *Proc. of the AAAI Conf. on Artificial Intelligence*, vol. 35, no. 12, pp. 10 639–10 646, 2021.

[27] H. Krasowski, J. Thumm, M. Müller, X. Wang, and M. Althoff, “Provably safe reinforcement learning: A theoretical and experimental comparison,” in <https://arxiv.org/abs/2205.06750>, 2022.

[28] J. F. Fisac, A. K. Akametalu, M. N. Zeilinger, S. Kaynama, J. Gillula, and C. J. Tomlin, “A general safety framework for learning-based control in uncertain robotic systems,” *IEEE Transactions on Automatic Control*, vol. 64, no. 7, pp. 2737–2752, 2019.

[29] O. Bastani, “Safe reinforcement learning with nonlinear dynamics via model predictive shielding,” in *Proc. of the American Control Conf. (ACC)*, 2021, pp. 3488–3494.

[30] S. Gros, M. Zanon, and A. Bemporad, “Safe reinforcement learning via projection on a safe set: How to achieve optimality?” in *21st IFAC World Congress*, vol. 53, 2020, pp. 8076–8081.

[31] K. P. Wabersich and M. N. Zeilinger, “A predictive safety filter for learning-based control of constrained nonlinear dynamical systems,” *Automatica*, vol. 129, p. 109597, 2021.

[32] G. Mason, R. Calinescu, D. Kudenko, and A. Banks, “Assured reinforcement learning with formally verified abstract policies,” ser. Proc. of the 9th Int. Conf. on Agents and Artificial Intelligence (ICAART), vol. 2, 2017, pp. 105–117.

[33] R. S. Sutton and A. G. Barto, *Reinforcement learning: An introduction*. MIT press, 2018.

[34] “Robotics - safety requirements - part 1: Industrial robots,” International Organization for Standardization, Geneva, CH, Standard DIN EN ISO 10218-1:2021-09 DC, Sep. 2021.

[35] C. Pek and M. Althoff, “Efficient computation of invariably safe states for motion planning of self-driving vehicles,” in *Proc. of the IEEE Int. Conf. on Intelligent Robots and Systems (IROS)*, 2018, pp. 3523–3530.

[36] S. Schepp, J. Thumm, S. B. Liu, and M. Althoff, “Sara: A tool for safe human–robot coexistence and collaboration through reachability analysis,” in *Proc. of the IEEE Int. Conf. on Robotics and Automation (ICRA)*, 2022, pp. 4312–4317.

[37] S. B. Liu, H. Roehm, C. Heinemann, I. Lütkebohle, J. Oehlerking, and M. Althoff, “Provably safe motion of mobile robots in human environments,” in *Proc. of the IEEE/RSJ Int. Conf. on Intelligent Robots and Systems (IROS)*, 2017, pp. 1351–1357.

[38] D. Beckert, A. Pereira, and M. Althoff, “Online verification of multiple safety criteria for a robot trajectory,” in *Proc. of the IEEE 56th Conf. on Decision and Control (CDC)*, 2017, pp. 6454–6461.

[39] P. F. Orzechowski, A. Meyer, and M. Lauer, “Tackling occlusions limited sensor range with set-based safety verification,” ser. Proc. of the IEEE Conf. on Intelligent Transportation Systems (ITSC), 2018, pp. 1729–1736.